International Journal of Engineering Science xxx (xxxx) 103744

Contents lists available at ScienceDirect

International Journal of Engineering Science

journal homepage: www.elsevier.com/locate/ijengsci

Resistivity contribution tensor for nonconductive sphere doublets

L. Lanzoni [a, c, d], E. Radi [b, c, *]

[a] Dipartimento di Ingegneria "Enzo Ferrari", Università di Modena e Reggio Emilia, Via Vivarelli, 10- 41125 Modena, Italy
[b] Dipartimento di Scienze e Metodi dell'Ingegneria, Università di Modena e Reggio Emilia, Via Amendola, 2 - 42122 Reggio Emilia, Italy
[c] Centro Interdipartimentale "En&Tech", via G. Amendola, 2, Reggio Emilia, 42122, Italy
[d] Centro Interdipartimentale "Crict", Via Vivarelli, 10- 41125 Modena, Italy

ARTICLE INFO

Keywords:
Sphere doublets
Tangent sphere coordinates
Stream function
Resistivity contribution tensor
Fourier heat conduction
Shooting method

ABSTRACT

The distribution of the temperature and heat flux fields around a couple of unequal nonconductive tangent spherical inhomogeneities (or pores) embedded in an infinite medium under a steady-state and remotely applied heat flux is addressed in the present work. Owing to the 3D geometrical layout of the inhomogeneity, use is made of the tangent sphere coordinate system. A corrective temperature field expressed in terms of convergent integrals is superposed to the fundamental one to fulfill the BCs at the surfaces of the spheres. When the heat flux is aligned to the symmetry axis (axisymmetric problem), the solution can be found straightforwardly by introducing a stream function, which allows for transforming the Neumann BCs into a Dirichlet boundary value problem. Conversely, for the transversal heat flux (non-axisymmetric problem), the problem is formulated in terms of temperature, thus leading to a system of two ODEs which is handled numerically through a Euler shooting method, after preliminary asymptotic expansions. Once the temperature fields are known, the components of the resistivity contribution tensor are assessed varying the aspect ratio of the two spheres. It is found that the extrema of the thermal resistivity are achieved for spheres of equal size. The study allows assessing the effective thermal conductivity of a wide range of smart composites involving insulating inhomogeneities resembling sphere doublets.

1. Introduction

A wide range of materials, ranging from natural rocks to sintered ceramics, smart composites, metamaterials, etc., involves inclusions or pores having particular shapes, which geometrical properties need to be accounted for to assess properly its performances. In particular, several experimental researches focus on the chance to impart specific physical properties to composites by driving the formation and growth of micro (or nano) inclusions into the background material, giving rise to optimized microstructures. Among such investigations, some concern the formation of dumbbell nanoparticles as basic components in colloidal crystals (e.g. Johnson et al., 2005) with anisotropic properties. As an example, starting from colloidal solution of monodisperse silica nanoparticles, new kinds of photonic materials can be obtained by following proper processes of synthesis (Park et al., 2010). The aspect ratio of such dumbbell-shaped nanoparticles depends upon the synthesis conditions. Methods of synthetization include centrifugation techniques of a solution of dispersed spherical nanoparticles, that leads to dumbbells (or triplets or, in some cases, larger clusters of spherical particles) having typically a dimension of some μm. Smaller particles, on the order of some tens of nanometers, can be obtained by exploiting

* Corresponding author.
E-mail address: eradi@unimore.it (E. Radi).

https://doi.org/10.1016/j.ijengsci.2022.103744
Received 15 April 2022; Received in revised form 11 July 2022; Accepted 10 August 2022
0020-7225/

chemical reactions starting from seed particles dispersed in microemulsions. This latter approach typically applies to silica colloids aimed at obtaining synthetic or hybrid (organic-inorganic) particles to realize optical sensors, photonic crystals and, in general, a new generation of smart composites (Kim et al., 2007). The possibility to obtain challenging microstructures for new functional materials is well elucidated in Wang et al. (2012).

Voids resembling sphere doublets can be observed also in austenitic stainless steel irradiated at certain temperature and pressure conditions (Porollo et al., 2006). It has been shown that nuclear radiations can drive void swelling and dislocation loops in steel and other metal alloys, thus affecting the microstructure of the material and, in turn, its short-term mechanical properties. Pore growth process, pore coalescence and pore interruption can be driven in Gasar metals to obtain a microstructure exhibiting specific physical and mechanical properties (Liu et al., 2018). In particular, by tailoring properly the synthesis conditions, the process of pore coalescence can be affected to obtain pores resembling a pair of bubbles characterized by different cross-sectional perimeter and aspect ratio. Challenging pore morphologies can be achieved by optimizing the solidification process.

Silica aerogels are nanoporous ultralight materials derived from a gel, in which the liquid component for the gel has been replaced with a gas, thus resulting in low density, high porosity synthetic materials. They present many interesting physical properties leading to several applications in the sector of building thermal insulation, due to their extremely low thermal conductivity. They are usually formed by spherical grains fused together into clusters and thus they are represented by regular packings of spheres in contact in order to define their effective thermal properties (e.g. He & Xie, 2015; Spagnol et al., 2008).

In recent applications, nanospherical particles are also added to fluids to increase their thermal conductivity. According to the thermal properties of the particles, the resulting suspensions, called nanofluids, are typically employed as heat transfer fluids due to their enhanced thermal conductivity compared to conventional liquids. A review on nanofluids modeling and applications was presented by Fan and Wang (2011) and Mahian, Kolsi and Amani (2019). The mechanisms of heat transfer enhancement of nanofluids have been studied by Pang, Jung and Kang (2014), who experimentally proved that the aggregation of nanoparticles can lead to the improvement of the thermal conductivity coefficient.

As known, the inhomogeneities embedded in a background matrix or dispersed in a fluid significantly affects the behavior of the composite or suspension. While a wide range of studies about the effective properties of materials containing spherical or ellipsoidal inclusions has been well developed, the same does not occur for inhomogeneities of different shape. On the other hand, adoption of "equivalent" ellipsoids to simulate inhomogeneities with challenging shape can leads to erroneous predictions (e.g. Kachanov & Sevostianov, 2018). For this motivation, some investigations have been recently addressed to evaluate the effective thermal and elastic properties of composites containing voids or rigid particles with some specific shape different from the ellipsoidal one.

The effects of various concave pore, cracks and helical inhomogeneities on the effective conductive properties of porous, cracked or reinforced materials have been investigated analytically and numerically by Chen et al., (2015); Sevostianov (2006); Sevostianov et al., (2016); Trofimov et al., (2017) and Trofimov and Sevostianov (2017) using various homogenization methods. Applicability of these results to overall conductivity of the porous rock and cathode material in Li-ion batteries has been discussed by Chen et al. (2017) and Vilchevskaya and Sevostianov (2020), respectively. Kushch and Sevostianov (2014) showed that shape, orientation, and spatial arrangement of the inhomogeneities in particulate composites may produce macroscopic anisotropy of the overall conductivity, whereas volume content of inhomogeneities yields the change in the anisotropy extent. Radi and Sevostianov (2016) and Lanzoni et al. (2018, 2020, 2022) worked out the components of the resistivity contribution tensor for insulating inhomogeneities having the shape of a torus as well as that two overlapping cylinders or spheres of arbitrary size. The analytical results were then compared with the predictions provided by equivalent spheroids, finding a reasonable agreement within a definite range of variation of the geometrical parameters. To examine the case where strong interactions between particles exist, the problem of two equal spheres in contact was investigated in Lanzoniet al. (2020) by using the tangent sphere coordinate system, as the limit case of two overlapping spheres. Moreover, the problem of two overlapping spheres of different sizes was recently solved in Lanzoni et al. (2022). The analysis was also extended to assess the effective elastic properties of composites containing rigid inhomogeneities with the shapes of a torus or two overlapping cylinders (Krasnitckii et al., 2019; Lanzoni et al., 2019). However, no results were provided up to now for the resistivity contribution tensor of two insulating spheres of different sizes touching each other in a single point.

The present work extends the number of investigations performed on the effective conductive properties of clusters of two insulating spheres. Indeed, it deals with the analytical and numerical evaluation of the overall thermal conductivity of a composite material or fluid containing pairs of nonconducting unequal touching spheres. The effective thermal property is assessed through the evaluation of the second-rank resistivity contribution tensor (Sevostianov & Kachanov, 2002), which gives the extra temperature variation related to the presence of the inhomogeneity embedded into the background matrix under a steady-state remotely applied heat flux. Owing to the geometrical layout of the inhomogeneity, reference is made to tangent sphere coordinates. The axisymmetric problem of a remotely applied heat flux acting along the symmetry axis of the insulating inhomogeneity is solved first by introducing a proper stream function (Section 3). This allows transforming the Neumann BCs at the surfaces of the spheres into a Dirichlet problem, thus leading to the temperature distribution in terms of a convergent series expansion. Then, the axial component of the resistivity contribution tensor is found in closed form by performing the heat flux vector across the surface of the spheres. The problem of a remote heat flux acting transversally to the symmetry axis of the inhomogeneity (skew problem) has been considered separately in Section 4. In such a case, the problem is directly formulated in terms of temperature as the stream function does not exist in this case. The temperature field encompasses the basic solution for a homogeneous medium and a corrective extra field due to the presence of the nonconductive inhomogeneity. Both terms are expressed in terms of convergent integrals. The condition of insulating spherical inhomogeneities leads to a couple of ODEs of second order for two unknown functions, with boundary conditions at both ends, which cannot be solved in closed form. However, an asymptotic analysis allows identifying the behavior of the unknown functions in the neighboring of the origin out of two unknown constants, as well as the exponential decaying at infinity. Therefore, a straightforward Euler

shooting procedure has been implemented for finding the two unknown constants, thus obtaining the temperature distribution around the two spheres and, in turn, the transverse components of the resistivity contribution tensor. The approach developed here for the 3D non-axisymmetric problem takes inspiration from the method proposed by O'Neill (1969) and then employed by Latta and Hess (1973), Davis (1977), Cox and Cooker (2000) and Lanzoni et al. (2020, 2022) for the case of two equal spheres, which has been generalized here to the problem of two spheres of different sizes.

The variation of the components of the resistivity contribution tensor as a function of the ratio between the radii of the two touching spheres is then provided, finding the extrema of both the components when the spheres have the same size. As discussed in Section 5, in such a situation the approximation given by "equivalent" prolate spheroids can lead to rough predictions, thus confirming the need to properly accounting for the actual geometry of the inclusions. Finally, concluding remarks are drawn in Section 6.

2. Formulation of the problem in tangent sphere coordinates

In this section, we derive the expressions for the resistivity contribution tensor components in the limiting case of two touching spheres with different diameters, namely D and D/ρ. We use the tangent sphere coordinate system (ξ, η, φ) sketched in Fig. 1 (see Moon and Spencer, 2012). Coordinate surfaces of this system are formed by toroids and spheres tangent to the xy coordinate plane at the origin. The tangent sphere coordinates are related to the Cartesian coordinates by the following relations

$$x = \frac{D\,\eta}{\xi^2+\eta^2}\cos\varphi, \qquad y = \frac{D\,\eta}{\xi^2+\eta^2}\sin\varphi, \qquad z = \frac{D\,\xi}{\xi^2+\eta^2}. \tag{2.1}$$

A constant value of ξ defines the surface of a sphere of radius $D/(2|\xi|)$ touching the origin of the coordinate system with the center laying on the z-axis at $z = D/(2\xi)$, for $0 \le \eta < \infty$ and $0 \le \varphi < 2\pi$. The surfaces of the two touching spheres of diameter D and D/ρ considered in the present section are defined by the coordinate $\xi = 1$ and $\xi = -\rho$, respectively, with $\rho > 0$.

The temperature distribution T under steady-state heat flux must satisfy the Laplace equation

$$\nabla^2 T = 0. \tag{2.2}$$

The heat flux then follows the isotropic Fourier law

$$\boldsymbol{q} = -k\nabla T, \tag{2.3}$$

where k is the heat conduction coefficient (W m^{-1} K^{-1}). Then, the insulating condition of vanishing normal heat flux on the surface of the two sphere requires

$$q_\xi = 0, \qquad \text{for} \quad \xi = 1, -\rho, \tag{2.4}$$

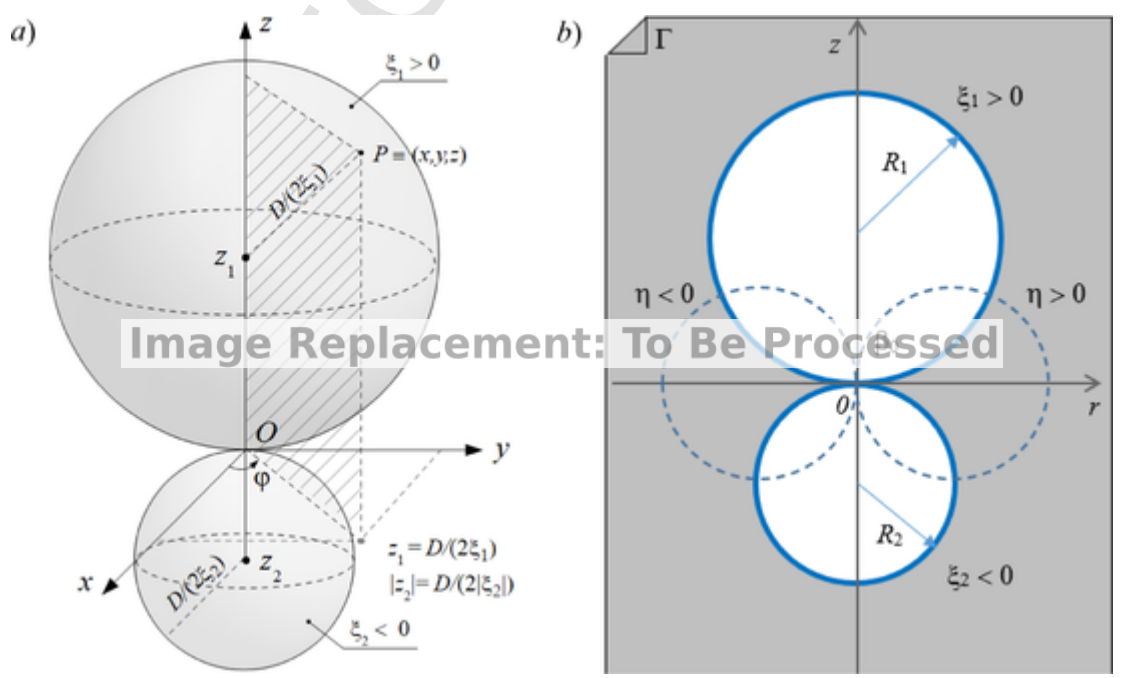

Fig. 1. *a*) Sketch of a sphere doublet referred to Cartesian (O, x, y, z) and toroidal (ξ, η, φ) coordinate systems and *b*) section of the sphere doublet in the rz plane.

and thus, from (2.11), on the surface of both spheres the temperature field must satisfy the Neumann boundary condition

$$\frac{\partial T}{\partial \xi} = 0, \qquad \text{at } \xi = 1 \text{ and } \xi = -\rho. \tag{2.5}$$

Far from the inhomogeneity (both ξ and η tend to zero) the heat flux must approach the unperturbed heat flux $\boldsymbol{q}_0$.

Let us calculate the temperature field and the components of the resistivity contribution tensor both for axial and transverse heat flux.

3. Heat flux along the symmetry axis (axisymmetric problem)

By introducing the stream function $\psi(\eta, \xi)$, the axisymmetric heat flux problem can be formulated as a Dirichlet boundary value problem.

The condition div $\boldsymbol{q} = 0$ allows for the following expression of the heat flux components in the tangent sphere coordinate system (see Eq. (A.2) in the Appendix)

$$q_\eta = -\frac{\left(\xi^2+\eta^2\right)^2}{\eta}\frac{\partial \psi}{\partial \xi}, \qquad q_\xi = \frac{\left(\xi^2+\eta^2\right)^2}{\eta}\frac{\partial \psi}{\partial \eta}. \tag{3.1}$$

Since the heat flux is irrotational (curl $\boldsymbol{q} = 0$), then the stream function ψ must satisfy the following equation (Fransaer et al., 1990, see also Eq. (A.3) in the Appendix for $q_\varphi = 0$)

$$\frac{\partial}{\partial \eta}\left(\frac{\xi^2+\eta^2}{\eta}\frac{\partial \psi}{\partial \eta}\right) + \frac{\partial}{\partial \xi}\left(\frac{\xi^2+\eta^2}{\eta}\frac{\partial \psi}{\partial \xi}\right) = 0. \tag{3.2}$$

We split the stream function onto the contribution ψ_0 induced by the uniform heat flux q_0 along the direction of the z-axis in a homogeneous medium and the corrective field ψ_1 due to the presence of the inhomogeneity as follows

$$\psi_0(\eta, \xi) = -\frac{q_0}{2}\left(\frac{\eta}{\xi^2+\eta^2}\right)^2, \tag{3.3}$$

$$\psi_1(\eta, \xi) = \frac{q_0}{2}\frac{\eta}{\sqrt{\xi^2+\eta^2}}\int_0^\infty \left[f_1(s)\sinh s\xi + f_2(s)\cosh s\xi\right] J_1(s\eta)\, ds, \qquad \text{for } -\rho \le \xi \le 1 \tag{3.4}$$

where J_1 is the Bessel function of the first kind of the first order. The function ψ_1 in (3.4) is the most general function satisfying Eq. (3.2) in the tangent sphere coordinates that is vanishing at $\eta = 0$ (Fransaer et al., 1990). The unknown functions $f_1(s)$ and $f_2(s)$ must be found by introducing $(3.1)_2$, (3.3) and (3.4) into the boundary condition (2.4).

By using $(3.1)_2$, the insulating boundary conditions (2.4) requires indeed

$$\frac{\partial \psi}{\partial \eta} = 0, \qquad \text{at } \xi = 1 \text{ and } \xi = -\rho. \tag{3.5}$$

Since the value of ξ along each of the two spherical surfaces is constant, it follows that the stream function must also be constant therein and the value of the constant is set equal to zero for simplicity, namely

$$\psi(\eta, 1) = 0, \qquad \psi(\eta, -\rho) = 0. \tag{3.6}$$

From these conditions, using the result 6.623.1 in Gradshteyn and Ryzhik (2007)

$$\int_0^\infty s\, e^{-s|\xi|} J_1(s\eta)\, ds = \frac{\eta}{\left(\xi^2+\eta^2\right)^{3/2}}, \tag{3.7}$$

one can obtain the following equations for the functions f_1 and f_2 introduced in (3.4)

$$f_1(s)\,\sinh s + f_2(s)\,\cosh s = s\, e^{-s}, \qquad -f_1(s)\sinh s\rho + f_2(s)\cosh s\rho = s\, e^{-s\rho}, \tag{3.8}$$

which admit the solution

$$f_1(s) = s\,\frac{\sinh[s(\rho-1)]}{\sinh[s(\rho+1)]}, \qquad f_2(s) = s\,-\frac{2s\,\sinh s\rho\,\sinh s}{\sinh[s(\rho+1)]}. \tag{3.9}$$

Therefore, the stream function becomes

$$\psi(\eta,\xi)=\frac{q_0}{2}\frac{\eta}{\sqrt{\xi^2+\eta^2}}\left\{-\frac{\eta}{\left(\xi^2+\eta^2\right)^{3/2}}+\int_0^\infty\frac{e^{(\xi+\rho-1)\,s}+e^{-(\xi+\rho-1)\,s}-e^{-(\xi+\rho+1)\,s}-e^{(\xi-\rho-1)\,s}}{2\sinh\left[(\rho+1)\,s\right]}\,s\,J_1(s\eta)\;ds\right\}. \tag{3.10}$$

By using the following Dirichlet series expansion

$$\frac{1}{\sinh\left[(\rho+1)\,s\right]}=\frac{2\,e^{-(\rho+1)\,s}}{1-e^{-2(\rho+1)\,s}}=2\sum_{n=0}^{\infty}e^{-(2n+1)(\rho+1)\,s}, \tag{3.11}$$

and the result

$$\int_0^\infty s\,e^{-a\,s}\cosh(bs)\;J_1(s\eta)\;ds=\frac{\eta}{2\left[(a-b)^2+\eta^2\right]^{3/2}}+\frac{\eta}{2\left[(a+b)^2+\eta^2\right]^{3/2}},$$

which holds for $a>b>0$ and follows from the derivative with respect to η of the integral (3.7), then the definite integral in (3.10) can be evaluated in closed form as

$$\int_0^\infty\frac{\cosh\left[(\xi+\rho-1)\,s\right]-e^{-(\rho+1)\,s}\cosh s\xi}{\sinh\left[(\rho+1)\,s\right]}\,s\,J_1(s\eta)\;ds=\sum_{n=0}^{\infty}\sum_{i=1}^{4}\frac{(-1)^{i-1}\eta}{\left[\left(\xi+\alpha_{in}\right)^2+\eta^2\right]^{3/2}}, \tag{3.12}$$

where

$$\begin{aligned}&\alpha_{1n}=2n(\rho+1)+2\rho,\\&\alpha_{2n}=2(n+1)(\rho+1),\\&\alpha_{3n}=-2n(\rho+1)-2,\\&\alpha_{4n}=-2(n+1)(\rho+1)=-\alpha_{2n}.\end{aligned} \tag{3.13}$$

The Fourier law for heat conduction in tangent sphere coordinates writes (Fransaer et al., 1990; Moon & Spencer, 2012, see also eqn (A.1) in the Appendix):

$$q_\eta=-\frac{k}{D}\left(\xi^2+\eta^2\right)\frac{\partial T}{\partial\eta},\qquad q_\xi=-\frac{k}{D}\left(\xi^2+\eta^2\right)\frac{\partial T}{\partial\xi}, \tag{3.14}$$

being k the (isotropic) thermal conductivity of the background material. Then, a comparison with Eq. (3.1) yields the following relations between temperature and stream functions

$$\frac{\partial T}{\partial\eta}=D\frac{\xi^2+\eta^2}{k\,\eta}\frac{\partial\psi}{\partial\xi},\qquad\frac{\partial T}{\partial\xi}=-D\frac{\xi^2+\eta^2}{k\,\eta}\frac{\partial\psi}{\partial\eta}. \tag{3.15}$$

By taking the derivative of ψ in (3.10) with respect to η, using Eqs (3.12) and $(3.15)_2$, one has

$$\frac{\partial T}{\partial\xi}=-D\frac{q_0}{k}\left\{\frac{\eta^2-\xi^2}{\left(\xi^2+\eta^2\right)^2}-\sum_{n=0}^{\infty}\sum_{i=1}^{4}(-1)^i\frac{2\eta^4-\eta^2\alpha_{in}\left(2\xi+\alpha_{in}\right)-2\xi^2\left(\xi+\alpha_{in}\right)^2}{2\sqrt{\xi^2+\eta^2}\left[\eta^2+\left(\xi+\alpha_{in}\right)^2\right]^{5/2}}\right\}, \tag{3.16}$$

and then integrating with respect to ξ, the following temperature distribution is obtained

$$T(\eta,\xi)=-D\frac{q_0}{k}\left\{\frac{\xi}{\xi^2+\eta^2}-\sqrt{\xi^2+\eta^2}\sum_{n=0}^{\infty}\sum_{i=1}^{4}\frac{(-1)^i\left[\eta^2+\xi\left(\xi+\alpha_{in}\right)\right]}{2\alpha_{in}\left[\eta^2+\left(\xi+\alpha_{in}\right)^2\right]^{3/2}}\right\}, \tag{3.17}$$

which satisfies also Eq. $(3.15)_1$ up to an arbitrary constant. It can be observed that the temperature distribution (3.17) satisfies the insulating boundary conditions (2.5).

The temperature distribution (3.17) is illustrated in Fig. 2*a*, whereas the corresponding heat flux is represented through contour lines in Fig. 2*b*, for $\rho=2$. As expected, going away from the inhomogeneity, the temperature field assumes a linear trend with the z coordinate according to the behavior of the basic temperature and, in turn, the heat flow approaches the unperturbed far field (0,0, q_0). Note also that the flow lines are tangent to the contour of the inhomogeneity, as required by the BCs. Fig. 3*a* and *b* display the dimensionless temperature distribution along the contour of the upper and lower spheres, respectively, from some values of the aspect ratio ρ. As expected, the extrema of the temperature values arise at the top ($\theta=\pi/2$) and at the bottom ($\theta=-\pi/2$) for both the spheres, being the applied heat flux aligned with the z axis. Moreover, as ρ increases, the temperature distribution on the contour of

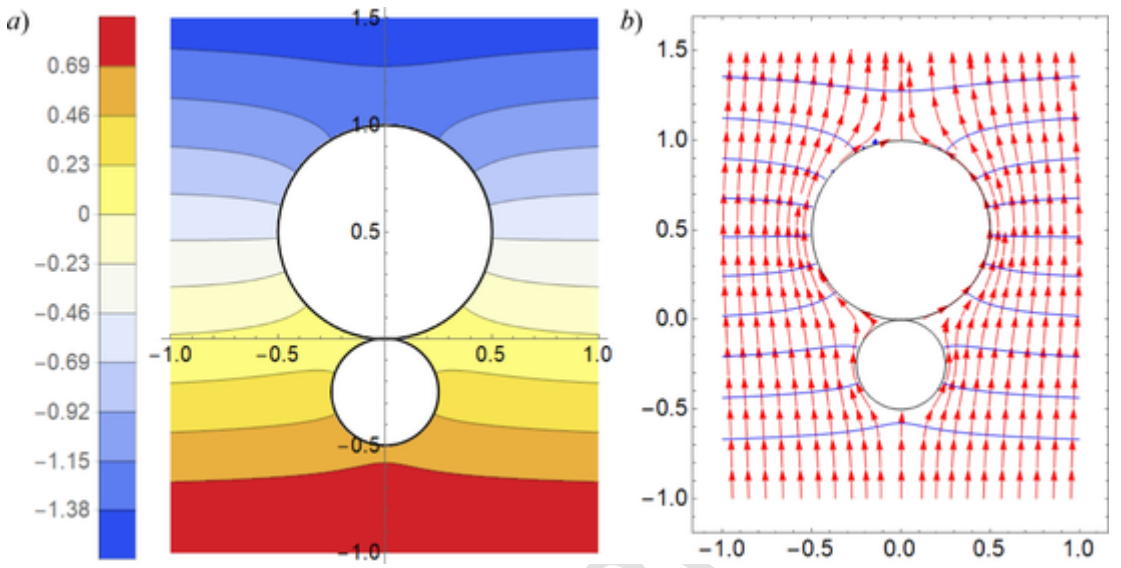

Fig. 2. Temperature and heat flow fields for $\xi_1 = 1$ and $\xi_2 = -2$ ($\rho = 2$) for a remote heat flux q_0 along the symmetry axis (axisymmetric problem).

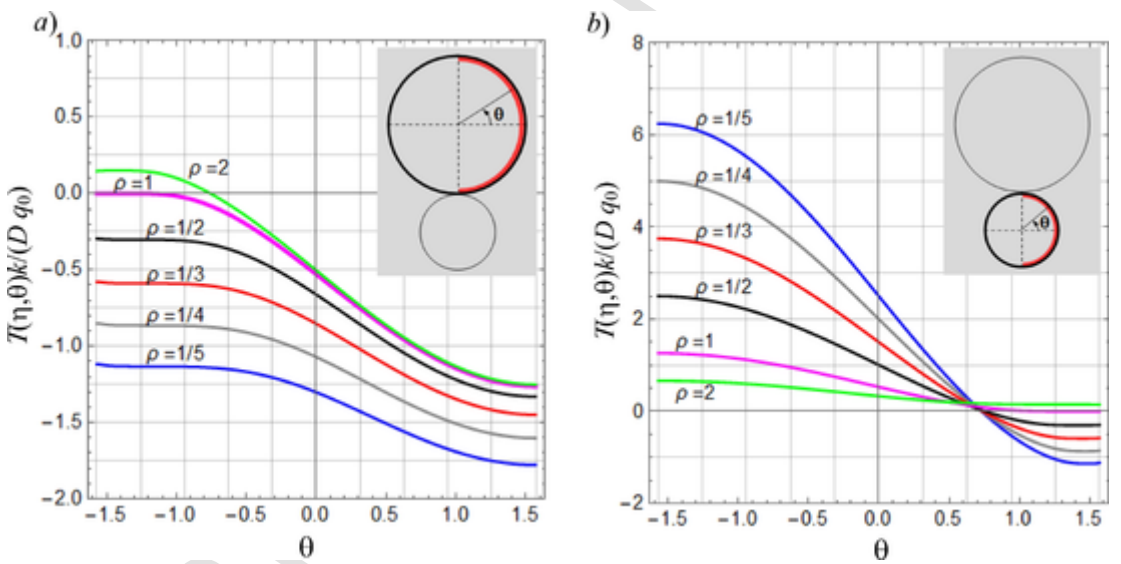

Fig. 3. Dimensionless temperature $T(\eta, \theta)\, k/(D\, q_0)$ along the contour of the *a*) upper sphere ($\xi = \xi_1 = 1$) and *b*) lower sphere ($\xi = \xi_2 = -\rho$) for some values of the aspect ratio ρ (axisymmetric problem).

the upper sphere (that defined by coordinate ξ_1) resembles the temperature distribution on the contour of a single nonconductive sphere with center (0, 0, $D/(2\,\xi_1)$) embedded in an infinite isotropic medium subjected to a remotely applied heat flux (0, 0, q_0):

$$T(\theta) = -\frac{q_0}{k}\frac{D}{2\xi_1}\left(1 + \frac{3}{2}\sin\,\theta\right).$$

The same behavior is retrieved at the surface of the lower sphere (that defined by coordinate $\xi = -\rho$) as $\rho \to 0$ ($D/\rho \to \infty$).

3.1. Axial component of the resistivity contribution tensor

The resistivity contribution tensor **R** for a pore or insulating inhomogeneity can be calculated using the relation:

$$\mathbf{R}\cdot\mathbf{q}_0 = \frac{1}{V_*}\int_S T\,\mathbf{n}\,dS, \tag{3.18}$$

where $\mathbf{q}_0$ is the remote heat flux vector, and V_* and S are the volume and surface of the two spheres, respectively. In particular, the component R_{33} can be calculated using the axisymmetric solution given in Section 6. The change in temperature gradient due to the insulating inhomogeneity bounded by surface $\xi = \xi_j$ $(j = 1, 2)$ is given by the surface integral

$$\phi = \sum_{j=1}^{2} \int_{S_j} T(\eta, \xi_j)\, \mathbf{n}\, dA, \tag{3.19}$$

where $\mathbf{n}$ is the outer unit normal on the inhomogeneity surfaces S_j $(j = 1, 2)$, being $\xi_1 = 1$ and $\xi_2 = -\rho$. Let $\boldsymbol{x} = (x, y, z)$ denote the position vector on the sphere surface, then (2.1) yields:

$$\mathbf{n}\, dA = (-1)^{j-1} \left[\frac{\partial \mathbf{x}}{\partial \eta} \times \frac{\partial \mathbf{x}}{\partial \varphi} \right]_{\xi=\xi_j} d\eta\, d\varphi = D^2 \frac{(-1)^{j-1}\eta}{\left(\xi^2+\eta^2\right)^3} \left[2\eta\, \xi\, \cos\varphi\, \mathbf{e}_\eta + 2\eta\, \xi\, \sin\varphi\, \mathbf{e}_\xi + \left(\xi^2-\eta^2\right) \mathbf{e}_\varphi \right] d\eta\, d\varphi, \tag{3.20}$$

where $\mathbf{e}_\eta$, $\mathbf{e}_\xi$ and $\mathbf{e}_\varphi$ are the unit vectors of the tangent sphere coordinate system. Therefore, the non-vanishing component of heat flux vector (3.19) across the upper half- inhomogeneity for remote heat flux directed along the symmetry axis is

$$\phi_z = -D^3 \frac{q_0}{k} \pi \sum_{j=1}^{2} (-1)^{j-1} \int_0^\infty \left\{ \frac{2\xi_j}{\left(\xi_j^2+\eta^2\right)^4} - \frac{1}{\left(\xi_j^2+\eta^2\right)^{5/2}} \sum_{n=0}^{\infty} \sum_{i=1}^{4} \frac{(-1)^i \left[\eta^2 + \xi_j\left(\xi_j + \alpha_{in}\right)\right]}{\alpha_{in} \left[\eta^2 + \left(\xi_j + \alpha_{in}\right)^2\right]^{3/2}} \right\} \left(\xi_j^2 - \eta^2\right)\, \eta\, d\eta,$$

namely

$$\phi_z = -D^3 \frac{q_0}{k} \frac{\pi}{3} \left\{ \frac{\rho^3+1}{2\rho^3} + \sum_{n=0}^{\infty} \sum_{i=1}^{4} (-1)^i \left[\frac{4\alpha_{in}^3 + \left(\alpha_{in}^3 - 6\alpha_{in}^2 - 12\alpha_{in} - 8\right)\left[\mathrm{sgn}(1+\alpha_{in}) - 1\right]}{\alpha_{in}^3(\alpha_{in}+2)^3} + \frac{4\alpha_{in}^3 + \left(\alpha_{in}^3 + 6\alpha_{in}^2\rho - 12\alpha_{in}\rho^2 + 8\rho^3\right)\left[\mathrm{sgn}(\rho-\alpha_{in}) - 1\right]}{\alpha_{in}^3(\alpha_{in}-2\rho)^3} \right] \right\}. \tag{3.21}$$

By calculating the finite sum for $i = 1, 2, 3, 4$ one has

$$\phi_z = \frac{q_0}{k} \frac{\pi D^3}{4(1+\rho)^3} \sum_{n=0}^{\infty} \left[\frac{2}{(n+1)^3} - \left(\frac{1+\rho}{1+n+n\rho} \right)^3 - \left(\frac{1+\rho}{\rho+n+n\rho} \right)^3 \right], \tag{3.22}$$

namely

$$\phi_z = \frac{q_0}{k} \frac{\pi D^3}{4(1+\rho)^3} \left[2\zeta(3) - \psi^{(2)}\left(\frac{1}{1+\rho} \right) - \psi^{(2)}\left(\frac{\rho}{1+\rho} \right) \right], \tag{3.23}$$

where ζ is the Riemann zeta function and $\psi^{(2)}$ is the second derivative of the digamma function ψ. Then, the axial component of the resistivity contribution tensor is

$$R_{zz} = \frac{\phi_z}{V_* q_0} = -\frac{3\rho^3}{4k\left(1+\rho^3\right)(1+\rho)^3} \left[2\zeta(3) - \psi^{(2)}\left(\frac{1}{1+\rho} \right) - \psi^{(2)}\left(\frac{\rho}{1+\rho} \right) \right], \tag{3.24}$$

where

$$V_* = \pi D^3 \frac{1+\rho^3}{6\rho^3}, \tag{3.25}$$

is the volume of the two tangent spheres. Note that for $\rho = 1$ then $R_{zz} = -1.3523/k$ and thus the result obtained by Lanzoni et al. (2020) for two equal touching spheres is fully recovered. Note also that, keeping fixed the thermal conductivity k, one has $R_{zz}(\rho) = R_{zz}(1/\rho)$ and that $k\, R_{zz} \to 3/2$ as $\rho \to 0, +\infty$, as predicted for a single sphere (Kachanov & Sevostianov, 2018).

4. Heat flux orthogonal to the symmetry axis (non-axisymmetric problem)

The non-axisymmetric problem defined by the heat flux orthogonal to the z-axis, namely $\boldsymbol{q}_0 = q_0\, \boldsymbol{e}_y$, is considered in the present section. Differently from the axisymmetric problem, in this case a stream function cannot be introduced. The problem is then formulated directly in terms of the temperature field $T = T_0 + T_1$, where, using Eq. $(2.1)_2$, the basic temperature T_0 is taken as

$$T_0(\eta, \xi, \varphi) = -\frac{q_0}{k} y = -\frac{q_0}{k} \frac{D\eta}{\xi^2+\eta^2} \sin\varphi, \tag{4.1}$$

and the corrective harmonic temperature field T_1 is assumed in the form

$$T_1(\eta,\xi,\varphi) = D\frac{q_0}{k}\sin\varphi\,\sqrt{\xi^2+\eta^2}\int_0^\infty \left[a(s)\ e^{s\xi} + b(s)\ e^{-s\xi}\right]\ J_1(s\eta)\ ds, \tag{4.2}$$

for $-\rho \le \xi \le 1$. The unknown functions $a(s)$ and $b(s)$ must be found by imposing the insulating boundary condition (2.4) at $\xi = 1$, $-\rho$, as reported hereinafter. They must be sought in such a way to make the corrective heat flux $\boldsymbol{q}_1 = -k\,\nabla T_1$ vanishing at infinity and finite everywhere. These conditions require the following asymptotic behavior of the unknown functions

$$a(0) = 0, \qquad b(0) = 0, \tag{4.3}$$

and

$$a(s) = o\left(s^{-1}\ e^{-s}\right), \qquad b(s) = o\left(s^{-1}\ e^{-\rho s}\right), \quad \text{as} \quad s \to \infty. \tag{4.4}$$

According to the assumptions of nonconducting inhomogeneities, the introduction of the temperature fields (4.1) and (4.2) in the insulating boundary condition (2.5) leads to

$$\frac{2\,\xi\,\eta}{\left(\xi^2+\eta^2\right)^{3/2}} + \xi\int_0^\infty \left[a(s)\ e^{s\xi} + b(s)\ e^{-s\xi}\right]\ J_1(s\eta)\ ds + \left(\xi^2+\eta^2\right)\int_0^\infty \left[a(s)\ e^{s\xi} - b(s)\ e^{-s\xi}\right]\ s\,J_1(s\eta)\ ds = 0. \tag{4.5}$$

By exploiting the following identity, which holds for the Bessel function J_1 (Gradshteyn & Ryzhik, 2007)

$$J_1(s\eta) = \frac{1}{s\,\eta^2}\left[\frac{J_1(s\eta)}{s} - \frac{d}{ds}\left(s\frac{dJ_1(s\eta)}{ds}\right)\right], \tag{4.6}$$

a double integration by parts of the last integral in Eq. (4.5) then yields

$$\begin{aligned}\eta^2\int_0^\infty s\ \left[a(s)\ e^{s\xi} - b(s)\ e^{-s\xi}\right]\ J_1(s\eta)\ ds = \\ = \int_0^\infty \left\{\frac{a(s)\,e^{s\xi}-b(s)\,e^{-s\xi}}{s} - \frac{d}{ds}\left[a(s)\ e^{s\xi} - b(s)\ e^{-s\xi}\right] - s\,\frac{d^2}{ds^2}\left[a(s)\ e^{s\xi} - b(s)\ e^{-s\xi}\right]\right\}\ J_1(s\eta)\ ds,\end{aligned} \tag{4.7}$$

being

$$\left[s\left[a(s)\ e^{s\xi} - b(s)\ e^{-s\xi}\right]\ \frac{dJ_1(s\eta)}{ds}\right]_0^\infty = 0, \qquad \left[sJ_1(s\eta)\ \frac{d}{ds}\left[a(s)\ e^{s\xi} - b(s)\ e^{-s\xi}\right]\right]_0^\infty = 0. \tag{4.8}$$

The introduction of (4.7) and the following result (Gradshteyn & Ryzhik, 2007, eqn 6.623.1)

$$\frac{2\xi\eta}{\left(\xi^2+\eta^2\right)^{3/2}} = 2\xi\int_0^\infty s\,e^{-s|\xi|}\ J_1(s\eta)\ ds, \tag{4.9}$$

in Eq. (4.5) then leads to a system of two ODEs of second order for the unknown functions $a(s)$ and $b(s)$, namely

$$\begin{aligned}&a(s) - (1+2s)\ s\,a'(s) - s^2a''(s) - \left[b(s) - s\,(1-2s)\ b'(s) - s^2b''(s)\right]\ e^{-2s} = -2s^2e^{-2s}, \\ &\left[a(s) - (1-2\rho s)\ s\,a'(s) - s^2a''(s)\right]\ e^{-2\rho s} - b(s) + s\,(1+2\rho s)\ b'(s) + s^2b''(s) = 2s^2\rho\,e^{-2\rho s}.\end{aligned} \tag{4.10}$$

The ODE system (4.10) with the boundary conditions (4.3) and (4.4) cannot be solved in closed form. However, to properly handle a numerical solution of system (4.10), it is helpful to find the asymptotic behavior of the solution both for $s \to 0$ and $s \to \infty$. In particular, let us denote with a_0 and b_0 the asymptotic behavior of functions a and b as $s \to 0$, then the system (4.10) provides

$$\begin{aligned}\left[a_0(s) - s\,a'_0(s) - s^2a''_0(s)\right]\ e^{-2\rho s} - \left[b_0(s) - s\,b'_0(s) - s^2b''_0(s)\right] = 2s^2\rho\,e^{-2\rho s}, \\ \left[a_0(s) - s\,a'_0(s) - s^2a''_0(s)\right]\ e^{-2\rho s} - \left[b_0(s) - s\,b'_0(s) - s^2b''_0(s)\right] = 2s^2\rho\,e^{-2\rho s},\end{aligned} \tag{4.11}$$

as $s \to 0$. From (4.11) it follows

$$\begin{aligned}a_0(s) - s\,a'_0(s) - s^2a''_0(s) \cong -\frac{2s^2\left(1+\rho\,e^{-2\rho s}\right)}{e^{-2s}-e^{-2\rho s}}, \\ b_0(s) - s\,b'_0(s) - s^2b''_0(s) \cong -\frac{2s^2\left(\rho+e^{-2s}\right)}{e^{-2s}-e^{-2\rho s}},\end{aligned} \tag{4.12}$$

as $s \to 0$. The inhomogeneous Euler ODEs (4.12) admit the following exact solutions for the functions a_0 and b_0 satisfying the boundary conditions (4.3)

$$
\begin{aligned}
a_0(s) &= \frac{1}{4s(\rho+1)^3}\left[e^{-2s}\Phi\left(e^{-2(\rho+1)s},\ 3,\ \frac{1}{1+\rho}\right)+\ \rho\ Li_3\left(e^{-2(\rho+1)s}\right)-\rho\,\zeta(3)+\frac{1}{2}\psi^{(2)}\left(\frac{\rho}{1+\rho}\right)+\pi\left(\csc\frac{\rho\,\pi}{1+\rho}\right)^2\left(\pi^2\cot\frac{\rho\,\pi}{1+\rho}-s^2(1+\rho)^2\sin\frac{2\rho\,\pi}{1+\rho}\right)\right] \\
&\quad+\frac{1}{2(\rho+1)^2}\left[e^{-2s}\Phi\left(e^{-2(\rho+1)s},\ 2,\ \frac{1}{1+\rho}\right)+\rho\ Li_2\left(e^{-2(\rho+1)s}\right)\right]+A_0\,s, \\
b_0(s) &= \frac{1}{4s(\rho+1)^3}\left[e^{-2\rho s}\rho\,\Phi\left(e^{-2(\rho+1)s},\ 3,\ \frac{\rho}{1+\rho}\right)+\ Li_3\left(e^{-2(\rho+1)s}\right)-\ \zeta(3)+\frac{\rho}{2}\psi^{(2)}\left(\frac{1}{1+\rho}\right)+\pi\,\rho\left(\csc\frac{\pi}{1+\rho}\right)^2\left(\pi^2\cot\frac{\pi}{1+\rho}-s^2(1+\rho)^2\sin\frac{2\,\pi}{1+\rho}\right)\right] \\
&\quad+\frac{1}{2(1+\rho)^2}\left[e^{-2\rho s}\rho\ \Phi\left(e^{-2(\rho+1)s},\ 2,\ \frac{\rho}{1+\rho}\right)+\ Li_2\left(e^{-2(\rho+1)s}\right)\right]+B_0\,s,
\end{aligned}
\tag{4.13}
$$

where A_0 and B_0 are unknown constants, Φ, Li_n and $\psi^{(n)}$ denote the Lerch transcendent function, the polylogarithm function, and the n-th derivative of the digamma function ψ, respectively (Erdélyi et al., 1981).

On the other hand, as $s \to \infty$ one has from (4.10)

$$
\begin{aligned}
&a_\infty(s) - s\,a'_\infty(s) - 2s^2 a'_\infty(s) - s^2 a''_\infty(s) = -2s^2 e^{-2s}, \\
&b_\infty(s) - s\,b'_\infty(s) - 2s^2\rho b'_\infty(s) - s^2 b''_\infty(s) = -2\rho\,s^2 e^{-2\rho s}.
\end{aligned}
\tag{4.14}
$$

The solutions of the two homogeneous ODEs (4.14) satisfying the boundary conditions (4.4) then provide the following asymptotic solution of the ODE system (4.10)

$$
a_\infty(s) = \left(-\frac{s}{2}+\frac{A_\infty}{s}\right)e^{-2s}+o\left(s^{-1}e^{-2s}\right),\qquad b_\infty(s) = \left(-\frac{s}{2}+\frac{B_\infty}{s}\right)e^{-2\rho s}+o\left(s^{-1}e^{-2\rho s}\right),\qquad \text{as } s\to\infty,
\tag{4.15}
$$

where A_∞ and B_∞ are unknown constants.

Since the coefficients multiplying the highest order derivative terms in the ODE system (4.10) are vanishing at $s = 0$, then the numerical integration of (4.10) must be started at $s = \varepsilon$, where $0 < \varepsilon << 1$. Therefore, the asymptotic solutions (4.13) will be used for defining the initial values of the unknown functions a and b and their derivatives at $s = \varepsilon$ in terms of the two unknown constants A_0 and B_0, namely

$$
a(\varepsilon) = a_0(\varepsilon),\qquad b(\varepsilon) = b_0(\varepsilon),\qquad a'(\varepsilon) = a'_0(\varepsilon),\qquad b'(\varepsilon) = b'_0(\varepsilon).
\tag{4.16}
$$

A shooting procedure is then performed on the values of A_0 and B_0 which yield exponentially decaying functions $a(s)$ and $b(s)$ as $s \to \infty$, according to the results (4.15) of the asymptotic analysis. In the numerical simulations, we assumed $\varepsilon = 0.01$ and then we impose vanishing of functions $a(s)$ and $b(s)$ at $s = 10^2$. Such values reveal adequate for all the aspect ratio ρ hereinafter investigated. In particular, for $\rho = 2$, $a(\varepsilon) = 1.78574$, $b(\varepsilon) = 2.51386$, $a'(\varepsilon) = 0.494486$, $b'(\varepsilon) = 0.494453$ and a constant step size equals to $5 \cdot 10^{-6}$ has been used to handle the shooting scheme, funding satisfactory accuracy.

The temperature distribution in the material for $\varphi = \pi/2$ is plotted in Fig. 4a, whereas the corresponding heat flux is represented in Fig. 4b for $\rho = 2$. Similarly to the axisymmetric problem, also in this case the flow lines of the heat flux surround the contour of the

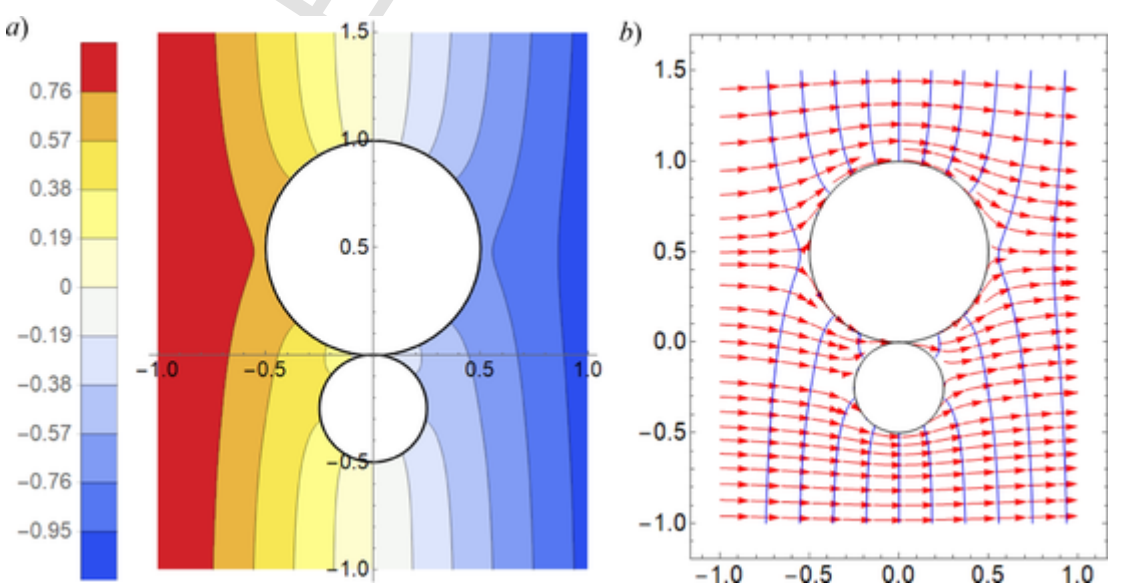

Fig. 4. Dimensionless temperature and heat flow fields for $\xi_1 = 1$ and $\xi_2 = -2$ ($\rho = 2$) for a remote heat flux $\boldsymbol{q}_0$ along the direction normal to the symmetry axis (non-axisymmetric problem).

spheres, and they become parallel to the *y* axis moving away from the origin. This confirms that the perturbation vanishes at infinity and, in turn, that the basic solution is retrieved there.

The variation of the dimensionless temperature field along the contour of the spheres is plotted in Fig. 5. Since the applied heat flux is aligned transversally to the symmetry axis, for both the spheres the extrema of the temperature take place near of the points furthest from the *z* axis, namely for $\theta \cong 0$. Note that, as ρ decreases, the stationary points on the upper sphere tend to go towards the *xy* plane, whereas they tend to move away from it for the lower sphere. Moreover, similarly to the case of the heat flux aligned with the symmetry axis, as ρ increases (decreases), the temperature distribution on the contour of the upper (lower) sphere resembles that found for an insulating single sphere embedded in an infinite medium under the action of a transverse remotely applied heat flux (q_0, 0, 0), namely:

$$T(\theta) = -D\frac{q_0}{k}\frac{\cos\theta}{2\rho}.$$

4.1. Transversal component of the resistivity contribution tensor

The substitution of the total temperature field $T = T_0 + T_1$ given by equations (6.20) and (6.21) into (6.31), yields the transversal component of the heat flux across the two spherical surfaces $\phi_y = \phi_y^{(0)} + \phi_y^{(1)}$, where

$$\phi_y^{(0)} = -2\pi D^3\frac{q_0}{k}\int_0^\infty\left[\frac{1}{\left(1+\eta^2\right)^4}+\frac{\rho}{\left(\rho^2+\eta^2\right)^4}\right]\eta^3 d\eta = -\pi D^3\frac{q_0}{k}\frac{1+\rho^3}{6\rho^3}, \tag{4.18}$$

and

$$\phi_y^{(1)} = 2\pi D^3\frac{q_0}{k}\int_0^\infty\eta^2 d\eta\int_0^\infty\left[\frac{a(s)e^s+b(s)e^{-s}}{\left(1+\eta^2\right)^{5/2}}+\rho\frac{a(s)e^{-\rho s}+b(s)e^{\rho s}}{\left(\rho^2+\eta^2\right)^{5/2}}\right]J_1(s\eta)\ ds, \tag{4.19}$$

namely

$$\phi_y^{(1)} = \frac{2}{3}\pi D^3\frac{q_0}{k}\int_0^\infty\left[\left(1+e^{-2\rho s}\right)a(s)+\left(1+e^{-2s}\right)b(s)\right]s\ ds, \tag{4.20}$$

being

$$\int_0^\infty\frac{\eta^2 J_1(s\eta)}{\left(\rho^2+\eta^2\right)^{5/2}}d\eta = \frac{s\,e^{-\rho s}}{3\rho}. \tag{4.21}$$

The numerical calculation of the definite integral in (4.20) is performed using the numerical solution of the ODE system (4.11). Therefore, the transversal component of the resistivity contribution tensor is

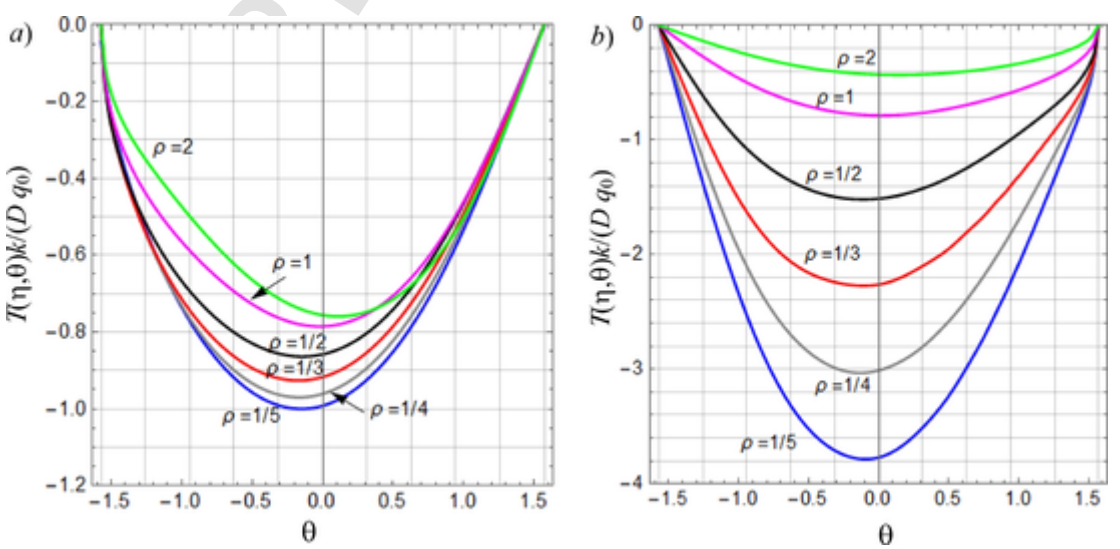

Fig. 5. Dimensionless temperature $T(\eta, \theta)\, k/(D\, q_0)$ along the contour of the *a*) upper sphere ($\xi = \xi_1 = 1$) and *b*) lower sphere ($\xi = \xi_2 = -\rho$) for some values of the aspect ratio ρ (non-axisymmetric problem).

$$R_{yy} = \frac{\phi_y^{(1)} + \phi_y^{(2)}}{V_* \, q_0}, \tag{6.35}$$

where V_* is the volume of the double spherical cavity defined in (3.25).

The variation of both the components R_{yy} (or R_{xx}) and R_{zz} of the resistivity contribution tensor with the ratio ρ is shown in Fig. 6. As expected, R_{yy} and R_{zz} tend to 3/2 as $\rho \to \infty$, thus recovering the known result for a single sphere. The extrema of both the components occur for two equal spheres. In detail, for $\rho = 1$, it is found $R_{yy} \cong 1.617$ and $R_{zz} \cong 1.352$.

5. Approximation by spheroidal inhomogeneities

The results obtained above in terms of the components R_{yy} and R_{zz} of the resistivity contribution tensor are here compared with those of spheroidal inhomogeneities of the aspect ratio $\beta = b_s / a_s$, where a_s is the radius of the spheroid in the xy plane and b_s is the semi-axis of the spheroid along the z-axis. In particular, for a single nonconducting spheroid one has (Kachanov & Sevostianov, 2018)

$$k\,R_{xx} = k\,R_{yy} = -\frac{1}{1-f_0}, \qquad kR_{zz} = -\frac{1}{2f_0}, \tag{5.1}$$

where

$$f_0 = \frac{\widehat{\rho}^2\,(1-g)}{2\left(\widehat{\rho}^2 - 1\right)}, \qquad g(\beta) = \begin{cases} \dfrac{1}{\beta\sqrt{1-\beta^2}} \arctan\dfrac{\sqrt{1-\beta^2}}{\beta}, & \text{oblate shape } (\beta<1) \\ \dfrac{1}{2\beta\sqrt{\beta^2-1}} \ln\dfrac{\beta+\sqrt{\beta^2-1}}{\beta-\sqrt{\beta^2-1}}, & \text{prolate shape } (\beta>1) \end{cases}. \tag{5.2}$$

Therefore, the components of the resistivity contribution tensor for a couple of nonconductive spheres of different size with $\rho > 1$ can be reasonably approximated by the corresponding components calculated for an insulating prolate spheroid that has the same volume and the same height along the z axis of the inhomogeneity (namely, $2b_s = D(1 + \rho^{-1})$). It follows the radius of the spheroid in its aspect ratio as

$$a_s = D\sqrt{\frac{1+\rho^3}{4\rho^2\,(1+\rho)}}, \qquad \beta = \frac{b_s}{a_s} = \sqrt{\frac{(1+\rho)^3}{1+\rho^3}}. \tag{5.3}$$

Conversely, if the equivalent prolate spheroid is taken to have the same volume of the inhomogeneity and the radius equal to that of the largest sphere (namely, $a_s = D/2$), the half height b_s of the spheroid in its aspect ratio read

$$b_s = D\frac{1+\rho^3}{2\rho^3}, \quad \beta = \frac{b_s}{a_s} = 1 + \frac{1}{\rho^3}. \tag{5.4}$$

As shown in Fig. 6, the first assumption leads to rough predictions as the axial component R_{zz} is significantly underestimate whereas the transverse components R_{yy} (and R_{xx}) are highly overestimated with respect the exact formulation. Vice versa, according to Eq. (5.4), the adoption of equivalent prolate spheroids having the same radius of that of the major sphere leads to reasonably accu-

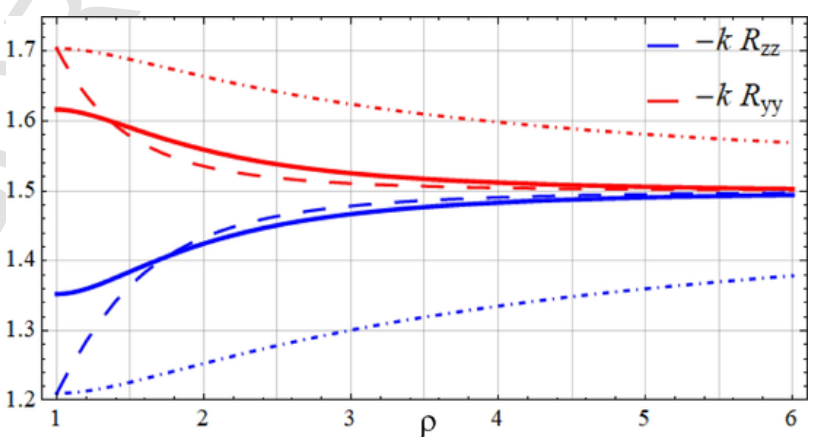

Fig. 6. Normalized variations of the components of the resistivity contribution tensor varying the ratio $\rho = R_1 / R_2$. Solid lines refer to touching spheres, whereas dash-dotted and dashed curves are provided by approximating spheroids with aspect ratios given by (5.3) and (5.4), respectively.

rate predictions for $\rho > 3/2$. In such cases, the approximated values of R_{zz} are slightly overrated whereas components R_{yy} (and R_{xx}) are slightly underrated with respect the results provided by the tangent sphere modelization. It is worth noticing that, for a couple of equal touching sphere (e.g. for $\rho \to 1$), the approximation through equivalent spheroids leads to incorrect predictions. This confirms the needing to accounting for the precise geometrical layout of this kind of inhomogeneities.

6. Concluding remarks

Temperature and heat flux fields around a inhomogeneity formed by a couple of unequal touching spheres embedded in an isotropic conductive matrix under an arbitrarily oriented and remotely applied steady state heat flux have been found in the present work. Then, the temperature distribution on the surfaces of the spheres has been used to assess the symmetric second-rank resistivity contribution tensor, which allows assessing the overall thermal conductivity of a composite embedding this kind of inhomogeneity according to the usual homogenization schemes (e.g. non-interaction approximation, Maxwell scheme, self-consistent approach, etc.). In particular, the variation of the principal components of the resistivity contribution tensor varying the aspect ratio of the inhomogeneity has been assessed, finding the extrema when the touching sphere take the same size ($\rho = 1$). The approximation provided by "equivalent" prolate spheroids having the same radius of the largest sphere (namely, $a_s = D / 2$) has been discussed also, finding good accuracy when the touching spheres are far to have the same size (let's say $\rho > 1.5$).

The present study completes a previous one about composites embedding nonconductive couples of unequal intersecting spheres, thus allowing to assess properly the effective thermal properties of composites with coalescing spherical during the entire coalescence process. Forthcoming works will be devoted to the evaluation of the overall elastic properties of materials containing inhomogeneities of the aforementioned shape.

Uncited references

Latta & Hess, 1973.

Declaration of Competing Interest

The authors declare that they have no known competing financial interests or personal relationships that could have appeared to influence the work reported in this paper.

Data Availability

Data will be made available on request.

Acknowledgments

L.L. and E.R. gratefully acknowledge the financial support by the Italian Ministry of Education, University and Research (MIUR) in the framework of the Project PRIN2020 "Opportunities and challenges of nanotechnology in advanced and green construction materials" (code 2020EBLPLS) and Project PRIN2020 "Mathematics for industry 4.0" (code 2020F3NCPX), respectively.

Appendix. Differential operators in tangent sphere coordinates

The gradient of a scalar function ψ and the divergence and curl of a vector field **q** in the tangent sphere coordinate system are (Moon & Spencer, 2012)

$$\nabla\psi = \frac{\xi^2+\eta^2}{D}\left(\frac{\partial\psi}{\partial\eta}\mathbf{e}_\eta + \frac{\partial\psi}{\partial\xi}\mathbf{e}_\xi + \frac{\partial\psi}{\partial\varphi}\mathbf{e}_\varphi\right), \tag{A.1}$$

$$\operatorname{div}\mathbf{q} = \frac{\left(\xi^2+\eta^2\right)^3}{D\,\eta}\left[\frac{\partial}{\partial\eta}\left(\frac{\eta\, q_\eta}{\left(\xi^2+\eta^2\right)^2}\right) + \eta\frac{\partial}{\partial\xi}\left(\frac{q_\xi}{\left(\xi^2+\eta^2\right)^2}\right)\right] + \frac{\xi^2+\eta^2}{D\,\eta}\frac{\partial q_\varphi}{\partial\varphi}, \tag{A.2}$$

$$\operatorname{curl}\mathbf{q} = \frac{\left(\xi^2+\eta^2\right)^2}{D\,\eta}\left\{\left[\frac{\partial}{\partial\xi}\left(\frac{\eta\, q_\varphi}{\xi^2+\eta^2}\right) - \frac{\partial}{\partial\varphi}\left(\frac{q_\xi}{\xi^2+\eta^2}\right)\right]\mathbf{e}_\eta + \left[\frac{\partial}{\partial\varphi}\left(\frac{q_\eta}{\xi^2+\eta^2}\right) - \frac{\partial}{\partial\eta}\left(\frac{\eta\, q_\varphi}{\xi^2+\eta^2}\right)\right]\mathbf{e}_\xi + \eta\left[\frac{\partial}{\partial\eta}\left(\frac{q_\xi}{\xi^2+\eta^2}\right) - \frac{\partial}{\partial\xi}\left(\frac{q_\eta}{\xi^2+\eta^2}\right)\right]\mathbf{e}_\varphi\right\}, \tag{A.3}$$

respectively, where $\mathbf{e}_\eta$, $\mathbf{e}_\xi$ and $\mathbf{e}_\varphi$ are the unit vectors of the tangent sphere coordinate system.

References

Chen, F., Popov, Y.A., Sevostianov, I., Romushkevich, R., Giraud, A., & Grgic, D. (2017). *Replacement relations for thermal conductivity of a porous rock. International Journal of Rock Mechanics and Mining Sciences, 97*, 64–74.

Chen, F., Sevostianov, I., Giraud, A., & Grgic, D. (2015). *Evaluation of the effective elastic and conductive properties of a material containing concave pores. International Journal of Engineering Science, 97*, 60–68.

Cox, S.J., & Cooker, M.J. (2000). *Potential flow past a sphere touching a tangent plane. Journal of Engineering Mathematics, 38*, 355–370.

Davis, A.M.J. (1977). *High frequency limiting virtual-mass coefficients of heaving half-immersed spheres*. *Journal of Fluid Mechanics*, *80*(2), 305–319.
Erdélyi, A., Magnus, W., Oberhettinger, F.& ., & Tricomi, F.G. (1981). *Higher transcendental functions*: *1*. New York: Krieger.
Fan, J., & Wang, L. (2011). *Review of heat conduction in nanofluids*. *The Journal of Heat Transfer-T ASME*, *133*, 040801.
Fransaer, J., De Graef, M., & Roos, J. (1990). *The temperature distribution around a spherical particle on a planar surface*. *The Journal of Heat Transfer*, *112*, 561–566.
Gradshteyn, I.S., & Ryzhik, I.M. (2007). *Table of integrals, series, and products*. Elsevier.
He, Y.L., & Xie, T. (2015). *Advances of thermal conductivity models of nanoscale silica aerogel insulation material*. *Applied Thermal Engineering*, *81*, 28–50.
Johnson, P.M., van Kats, C.M., & van Blaaderen, A. (2005). *Synthesis of colloidal silica dumbbells*. *Langmuir : The ACS journal of surfaces and colloids*, *21*, 11510–11517.
Kachanov, M., & Sevostianov, I. (2018). *Micromechanics of materials, with applications*. Springer.
Kim, J.-.J., Shin, K., & Suh, K.-.D. (2007). *Preparation of organic-inorganic doublet particles using seeded polymerization*. *Macromolecular Research*, *15*(7), 601–604.
Krasnitckii, S., Trofimov, A.L., Radi, E., & Sevostianov, I. (2019). *Effect of a rigid toroidal inhomogeneity on the elastic properties of a composite*. *Mathematics and Mechanics of Solids*, *24*, 1129–1146.
Kushch, V.I., & Sevostianov, I. (2014). *Dipole moments, property contribution tensors and effective conductivity of anisotropic particulate composites*. *International Journal of Engineering Science*, *74*, 15–34.
Lanzoni, L., Radi, E., & Sevostianov, I. (2018). *Effect of cylindrical fibers, with cross-sections formed by two circular arcs, on the overall conductivity of a composite*. *International Journal of Solids and Structures*, *138*, 264–276.
Lanzoni, L., Radi, E., & Sevostianov, I. (2019). *Effect of pair coalescence of circular pores on the overall elastic properties*. *International Journal of Solids and Structures*, *172*, 38–50.
Lanzoni, L., Radi, E., & Sevostianov, I. (2020). *Effect of spherical pores coalescence on the overall conductivity of a material*. *Mechanics of Materials*, *148*, 103463.
Lanzoni, L., Radi, E., & Sevostianov, I. (2022). *Resistivity contribution tensor for two nonconductive overlapping spheres having different radii*. Mathematics and Mechanics of Solids. doi:10.1177/10812865221108373.
Latta, G.E., & Hess, G.B. (1973). *Potential flow past a sphere tangent to a plane*. *Physics of Fluids*, *16*, 974–976.
Liu, X., Li, Y., Wang, J., & He, Y. (2018). *The pore growth process and pore coalescence process in Gasar copper*. *Materials Characterization*, *137*, 231–243.
Mahian, O., Kolsi, L., Amani, M., et al. (2019). *Recent advances in modeling and simulation of nanofluid flows-part I: Fundamentals and theory*. *Physics Reports*, *790*, 1–48.
Moon, P., & Spencer, D.E. (2012). *Field theory handbook: Including coordinate systems, differential equations and their solutions*. Springer.
O'Neill, M.E. (1969). *On asymmetrical slow viscous flows caused by the motion of two equal spheres almost in contact*. *Proceedings of the Cambridge Philosophical Society*, *65*, 543–556.
Pang, C., Jung, J.Y., & Kang, Y.T. (2014). *Aggregation based model for heat conduction mechanism in nanofluids*. *International Journal of Heat and Mass Transfer*, *72*, 392–399.
Park, J.-.G., Forster, J.D., & Dufresne, E.R. (2010). *High-yield synthesis of monodisperse dumbbell-shaped polymer nanoparticles*. *Journal of the American Chemical Society*, *132*, 5960–5961.
Porollo, S.I., Dvoriashin, A.M., Konobeev, Yu.V., Ivanov, A.A., Shulepin, S.V., & Garner, .A. (2006). *Microstructure and mechanical properties of austenitic stainless steel 12X18H9T after neutron irradiation in the pressure vessel of BR-10 fast reactor at very low dose rates*. *Journal of Nuclear Materials*, *359*, 41–49.
Radi, E., & Sevostianov, I. (2016). *Toroidal insulating inhomogeity in an infinite space and related problems*. *Proceedings of the Royal Society A*, *472*, 20150781.
Sevostianov, I. (2006). *Thermal conductivity of a material containing cracks of arbitrary shape*. *International Journal of Engineering Science*, *44*(8–9), 513–528.
Sevostianov, I., Chen, F., Giraud, A., & Grgic, D. (2016). *Compliance and resistivity contribution tensors of axisymmetric concave pores*. *International Journal of Engineering Science*, *101*, 14–28.
Sevostianov, I., & Kachanov, M. (2002). *Explicit cross-property correlations for anisotropic two-phase composite materials*. *Journal of Mechanics and Physics Solids*, *50*, 253–282.
Spagnol, S., Lartigue, B., Trombe, A., & Gibiat, V. (2008). *Modeling of thermal conduction in granular silica aerogels*. *Journal of Sol-Gel Science and Technology*, *48*(1), 40–46.
Trofimov, A., Drach, B., Kachanov, M., & Sevostianov, I. (2017). *Effect of a partial contact between the crack faces on its contribution to overall material compliance and resistivity*. *International Journal of Solids and Structures*, *108*, 289–297.
Trofimov, A., & Sevostianov, I. (2017). *The effect of waviness of a helical inhomogeneity on its stiffness- and conductivity contribution tensors*. *International Journal of Engineering Science*, *116*, 145–154.
Vilchevskaya, E., & Sevostianov, I. (2020). *Effect of pore shapes on the overall electrical conductivity of cathode material in Li-ion batteries*. *International Journal of Engineering Science*, *146*, 103187.
Wang, Y., Wang, Y., Breed, D.R., Manoharan, V.N., Feng, L., Hollingsworth, A.D., … Pine, D.J. (2012). *Colloids with valence and specific directional bonding*. *Nature*, *491*, 51–54.